frontiers | Frontiers in Sensors

TYPE Original Research
PUBLISHED 18 October 2022
DOI 10.3389/fsens.2022.1037723

OPEN ACCESS

EDITED BY
Chang-Hyung Choi,
Daegu Haany University, South Korea

REVIEWED BY
Heon-Ho Jeong,
Chonnam National University, South Korea
Sang Seok Lee,
Korea Institute of Science and Technology (KIST), South Korea

*CORRESPONDENCE
Huanan Wang,
huananwang@dlut.edu.cn

SPECIALTY SECTION
This article was submitted to Lab-on-a-Chip Devices,
a section of the journal
Frontiers in Sensors

RECEIVED 06 September 2022
ACCEPTED 07 October 2022
PUBLISHED 18 October 2022

CITATION
Zhang H, Li C, Zhang Y, An C, Li H, Yu J, Zhang Y, He W and Wang H (2022), High-throughput generation of microfluidic-templating microgels for large-scale single-cell encapsulation. *Front. Sens.* 3:1037723.
doi: 10.3389/fsens.2022.1037723

High-throughput generation of microfluidic-templating microgels for large-scale single-cell encapsulation

Haoyue Zhang[1], Chengze Li[1], Yujie Zhang[1], Chuanfeng An[1,2,3], Hanting Li[1], Jiahui Yu[1], Yonghao Zhang[1], Wei He[1] and Huanan Wang[1]*

[1]Key State Laboratory of Fine Chemicals, School of Bioengineering, Dalian University of Technology, Dalian, China, [2]Guangdong Key Laboratory for Biomedical Measurements and Ultrasound Imaging, School of Biomedical Engineering, Health Science Center, Shenzhen University, Shenzhen, China, [3]Central Laboratory, Longgang District People's Hospital of Shenzhen and The Second Affiliated Hospital of The Chinese University of Hong Kong, Shenzhen, China

Microfluidics-based fabrication of cell-laden microgels has shown great potential for applications in cell therapy and tissue engineering, however, the difficulty in chip operation and compromised cell viability due to cell sedimentation and channel blockage remain a major challenge for functional cell-laden microgels preparation. Herein, we presented the design and optimization of integrated microfluidic chip for large-scale preparation of cell-laden microgels with controllable size and complex microstructure. Specifically, to avoid severe cell sedimentation and uneven distribution in the parallelized microchannel, we simulated cell movement state using computational fluid dynamics simulation. It was found that higher laminar flow velocity gradient and higher precursor viscosity can significantly improve the uniform cell distribution in parallelized channels and reduce the product difference between channels. Moreover, we designed multiple-layered microfluidic chips allowing multiple inputting liquids for the fabrication of microgels with complex structures. This integrated chip facilitated cell encapsulation at a maximum production rate of 240 ml/h of cell suspension with retained cell viability and functionality. Therefore, our study provided a biocompatible and high-throughput strategy for large-scale preparation of cell-laden microgels, which can enable significant advances for clinical-relevant applications of cell-laden microgels, including cell therapy, tissue regeneration and 3D bioprinting.

KEYWORDS

computational fluid dynamics simulation, microfluidic droplets, integrated microfluidic chip, alginate, cell-laden microgel

Introduction

Human tissues are typically composed of a considerably high density of cells that are resided in the extracellular matrix (ECM) and assembled in a hierarchical manner (Li et al., 2018). To replicate such highly cellularized constructs even at a single-cell resolution may render the engineered construct with tissue-specific biological functions (Zhao, 2013). This technique, however, requires a substantially large number of cellularized microtissue modules as building blocks (Martins et al., 2017; Li et al., 2018; Youn et al., 2020). To this end, microscopic hydrogels (microgels) encapsulated with live cells at single-cell level can serve as subunits to enable bottom-up assembly of highly cellularized tissue mimics, which may lead to a paradigm shift in the design and reconstruction of engineered tissue/organs (Li et al., 2018; Zhang et al., 2018; Mao et al., 2019). Moreover, microgels can further function as carriers for cell delivery to targets, and meanwhile, protect encapsulated allogeneic cells from rapid clearance by the host immune system (Mao et al., 2017; An et al., 2020; Zhang et al., 2022). All these applications rely on massive, large-scale of single-cell manipulation and encapsulation (Griffin et al., 2015; Griffin et al., 2020; Zhang et al., 2022), which has been proven to be extremely challenging considering the difficulties including 1) high probability of production device being blocked due to jamming of cells or microparticles (Li et al., 2018), 2) the difficulty to achieve monodispersity of the resulting droplets/microgels upon scale-up production (Martins et al., 2017), and 3) the request for the fabrication device to be mechanically robust so as to withstand high fluid pressure (Jeong et al., 2016; Li et al., 2018).

To achieve large-scale production of monodisperse cell-laden droplets or microparticles, extensive efforts have been made in the development of microfluidics-based strategies (Jeong et al., 2016; Martins et al., 2017). One of the recently proposed strategies is based on step emulsification, wherein droplet formation is driven by interfacial tension which can avoid the influence of the fluid fluctuation on the uniformity of the resulting droplets (Amstad et al., 2016; Stolovicki et al., 2017; Montessori et al., 2018). The advantages such as simple design of channel structure and mild fabrication process make it possible to realize large-scale production of droplets (Ofner et al., 2017; Hati et al., 2018). Nevertheless, this approach requires an extremely low flow velocity (less than 0.008 m/s (Stolovicki et al., 2017)) to ensure the droplet size independent from the flow rate, and it is also difficult to reduce the size of resulting droplets due to the influence of the viscosity of the disperse phase and the wettability of the channel surfaces; this makes it difficult for applications for cell encapsulation (Zhu and Wang, 2016; Montessori et al., 2018). An alternative strategy was to design integrated microfluidic chips with numerous parallelized drop-maker units (DMUs) (Nisisako and Torii, 2008; Romanowsky et al., 2012), which had the capacity of large-scale droplet/microparticle production with a production rate up to litters per hour (Jeong et al., 2015; Jeong et al., 2017; Yadavali et al., 2018). However, an intrinsic challenge in designing these integrated chips is to ensure equal distribution of liquid phase between all neighboring DMUs since the flow rate of the inputting liquid may attenuate after flowing through parallelized channels, which may lead to polydispersity of the resulting droplets (Romanowsky et al., 2012; Nawar et al., 2020). One common solution is to enlarge the dimension of the channels outside of DMUs to significantly lower the flow rate, thereby alleviating the decay of flow rate in each DMU (Conchouso et al., 2014; Femmer et al., 2015). This, however, may lower the flow velocity (less than 0.1 m/s (Nisisako et al., 2012)) of the liquid phase in those channels and increase the probability of channel blockage when cells or solidified microgels are introduced (Li et al., 2018). Our previous work has presented a microfluidic droplet-based strategy for large-scale production of cell-laden microgels by substantially increase the input flow rate while maintaining uniform liquid-phase distribution (Zhang et al., 2022). Although high fluid velocity can retard particle sedimentation and lower down the change of channel blockage, the aggregation of microparticles in long-distance transport is still difficult to be addressed (Khan et al., 2018; Li et al., 2018), which may compromise the bioactivity of the bioactive cargoes and hinder further high-throughput applications. Therefore, there is an imperative demand to develop techniques to improve the scalability and performance of recently developed high-throughput microfluidic techniques for the fabrication of cell-laden microgels with retained cell viability and precise control over preparation parameters.

Herein, we designed and optimized a strategy of microfluidic integration for large-scale generation of cell-laden microgels (Figures 1A,B). We explored the underlying mechanism of cell sedimentation during the encapsulation process and presented an optimized integrated microchannel design to achieve the substantial large-scale preparation of cell-laden microgels. We revealed the boundary conditions for cell deposition with laminar flow, and optimized the operation parameters *via* computational fluid dynamics (CFD) simulation to alleviate cell sedimentation and possible channel blockage. These findings guided us to optimize and design an integrated microfluidic chip containing multiple independent DMUs (Figures 1C,D); this chip can reach a production rate of 240 ml aqueous disperse phase per hour. We further demonstrated that this microfluidic approach can achieve large-scale production of cell-laden microgels with retained viability and long-term functionality of the encapsulated cells. In general, our study provided a biocompatible and high-throughput strategy for large-scale preparation of cell-laden microgels, which can enable significant advances for clinical-relevant applications of cell-laden microgels, including cell therapy, tissue regeneration and 3D bioprinting.

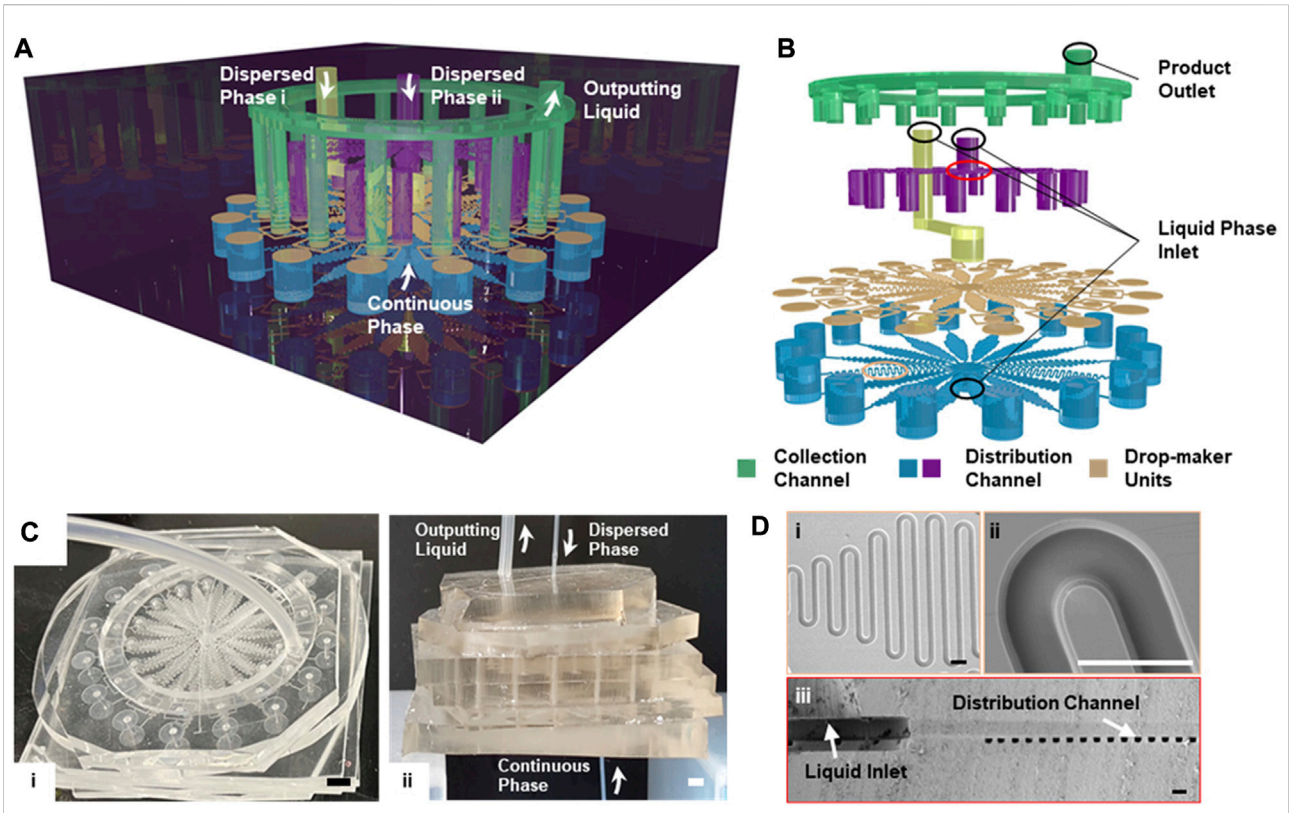

FIGURE 1
Schematic illustration of the integrated microfluid chip design **(A)** The multi-layered structure of the 16× DMUs integrated chip for structured microgels. **(B)** The stacked configuration of the microchannels within the integrated chip **(C)** Photograph showing the overall (i) and the side view (ii) of the integrated microfluidic chip containing DMUs with the channel width of 300 μm. Scale bar is 2 mm **(D)** The SEM image showing the overall (i) and detailed (ii) views of the distribution channel, and the cross-section of the liquid inlet and the distribution channel (iii). Scale bars are 100 μm.

Materials and methods

Materials

1H,1H,2H,2H-perfluoro-1-octanol (PFO), dimethyl sulfoxide (DMSO), arginine-glycine-aspartic acid (Arg-Gly-Asp, RGD), sodium alginate, 4-(2-hydroxyethyl) piperazine-1-ethanesulfonic acid (HEPES), dexamethasone, β-glycerophosphate are purchased from Sigma-Aldrich (United States). Minimal essential medium α (αMEM), fetal bovine serum (FBS), penicillin/streptomycin are purchased from Gibco (United States). Disodium-EDTA, lysis buffer, 1-ethyl (dimethylaminopropyl) carbodiimide (EDC), N-hydroxysulfosuccinimide (Sulfo-NHS) are purchased from Solarbio (China). Fluorocarbon oil (Novec 7,100 Engineered Fluid) is purchased from 3 M (USA). Nonionic fluorocarbon surfactant HN-surf is purchased from Momentive (United States). Polydimethylsiloxane (PDMS, RTV-615) is purchased from HUANOVA (China). Calcium chloride, ethylenediaminetetraacetic acid disodium salt (Na_2EDTA), sodium hydroxide, acetic acid and all the other chemicals are purchased from DAMAO (China).

Computational fluid dynamics simulations

Commercially available software (COMSOL Multiphysics, COMSOL Co.) was used to simulate fluid dynamics in the microfluidic channels of different geometry (designed by Auto CAD, Autodesk Inc.). The simulation was performed based on the following prerequisites: The minimal hydraulic pressure located at the outlet of the collection channel was set to zero so that the hydraulic pressure values throughout the chip can be normalized by the maximal pressure located at the inlet of aqueous phase. Thus, the values of local fluid resistance can be identical to that of fluid resistance which can be predicted by simulation. The flow rates of different liquids were used as inputting information for the simulation. As such, we can obtain the heat maps of the hydraulic pressure (or fluid resistance) and flow velocity throughout the chip by

simulation, in which hydraulic pressure was calculated by flow velocity at each position. The local fluid resistance and flow velocity for each DMU can be further quantified based on the heat maps. All CFD simulations based on the microfluidic chips of different geometries were performed using this setup.

Fabrication of Polydimethylsiloxane microfluidic devices

PDMS devices (Figure 1C) were fabricated by soft lithography protocol (Zhang et al., 2022). Negative photoresist SU-8 (MicroChem, USA) was spun coated onto a clean silicon wafer to thicknesses of 25, 50, 100, and 300 μm and then UV exposed through a mask (Newway, China) designed by CAD software (Art Service, United States). After developing the microstructure, a 10:1 mixture of Polydimethylsiloxane (PDMS, RTV-615, 3M, United States) and crosslinker were poured onto the pattern, and solidified overnight at 85°C. PDMS molds were peeled off the master and the channel inlets and outlets were made by using a 1 mm diameter biopsy punch (Wenhan, China). The PDMS replicas were bonded to a glass slide or another PDMS replica after oxygen-plasma activation of both surfaces and cured for 1 hour at 85°C. Hydrophobic silane Aquapel (PPG Industries, United States) was injected into the channel, incubated for 90 s at room temperature to render the channel surface hydrophobic. Finally, to totally remove Aquapel, all devices were incubated at 85°C for ~90 min.

Fabrication of microgels by integrated chips

For the large-scale generation of alginate microgels by integrated chips, the components of aqueous phases were containing 1 w/v % Na-alginate (Sigma, United States) and 50 mM Calcium-ethylenediaminetetraacetic acid (Ca-EDTA) complex as crosslinker. The same to the generation by single-channel devices. Fluorinated oil HFE7100 consisting of 0.1 v/v % acetic acid (DAMAO, China) and surfactant HN-surf were used as oil phase. Ca-EDTA complex was prepared by mixing calcium chloride (DAMAO, China) and disodium-EDTA (Solarbio, China) at a 1:1 M ratio, followed by pH neutralization to 7.4 using sodium hydroxide (DAMAO, China). All syringes were connected to the PDMS devices with polyethylene tubes with an inner diameter of 0.38 mm. The flow rates of aqueous (Q_{aqu}), oil (Q_{oil}) and buffering phases (Q_{buffer}) were individually controlled by different syringe pumps (lsp-1b, Longer, China). Q_{aqu} of each DMU was set at 50 μl/h for 25 μm channel, 100 μl/h for 50 μm channel, 200 μl/h for 75 μm channel, 400 μl/h for 100 μm channel, 1600 μl/h for 300 μm, 7500 μl/h for 500 μm and 15000 μl/h for 700 μm channel. Fast camera and optical microscope were used to monitor the formation and separation of microgels.

Fabrication of cell-laden microgels

For cell encapsulation, all devices were sterilized by washing with alcohol followed by UV illumination (λ−254 nm) for 3 h before use. Synthesis of Arg-Gly-Asp (RGD, Sigma, United States) conjugated alginate, isolation and culture of rat MSCs were realized according to previous report (An et al., 2020). Cells were dispersed in 1 w/v % alginate solution with a cell density of 2×10^6 cell/ml, and 50 mM Ca-EDTA. We used HFE7100 containing 5 v/v % PFO and 0.1 v/v % acetic acid as the oil phase. 25mM HEPES in minimal essential medium α (α-MEM, Thermo Fisher, United States) was used as the buffering phase to neutralize the acid and retreat encapsulated cells in aqueous phase. Integrated chip with 50 μm channel was used for cell encapsulation. For cell-laden spherical microgels preparation, Q_{aqu} for each DMU was kept constant at 100 ul/hr, Q_{oil} was set at 1,000 μl/h. For cell-laden Janus microgels preparation, Q_{aqu} for each aqueous phases injected into each DMU were kept constant at 50 ul/hr, Q_{oil} was set at 1,000 μl/h. For cell-laden core-shell microgels preparation, flow rate of shell phase Q_{shell} inject into each DMU was kept constant at 50 ul/hr, flow rate of core phase Q_{core} injected into each DMU was kept constant at 100 ul/hr, Q_{oil} was set at 1,000 μl/h. The cell-laden microgels were finally collected using a cell strainer followed by redispersion in cell culture media. The medium was refreshed every 3 days during *in vitro* cell culture. Cells in the microgels were cultured for 7 days. The cells were stained by DAPI nuclei staining (Thermo Fisher, United States). Fluorescent images were taken using a confocal laser scanning microscope (OLYMPUS FV1000, Japan).

Osteogenic differentiation of MSCs in microgels

To examine osteogenic differentiation of rat MSCs encapsulated in microgels, cell-laden microgels were cultured in osteogenic medium (α-MEM supplemented with 10 mM β-glycerophosphate, 50 μg/ml ascorbic acid, and 100 nM dexamethasone, all reagents purchased from Thermo Fisher, United States) and cultured for 21 days. SEM test samples were prepared by freeze-drying before scanning. SEM images were taken using a tungsten filament scanning electron microscope (FEI QUANTA 450, United States). After 21 days of culture, the osteogenic differentiation of MSCs was determined by alizarin red. Briefly, 500 μl of 2% alizarin red solution (pH = 4.2) was added into the sample and incubated for 5 min. Finally, samples were washed with distilled water until discoloration was complete.

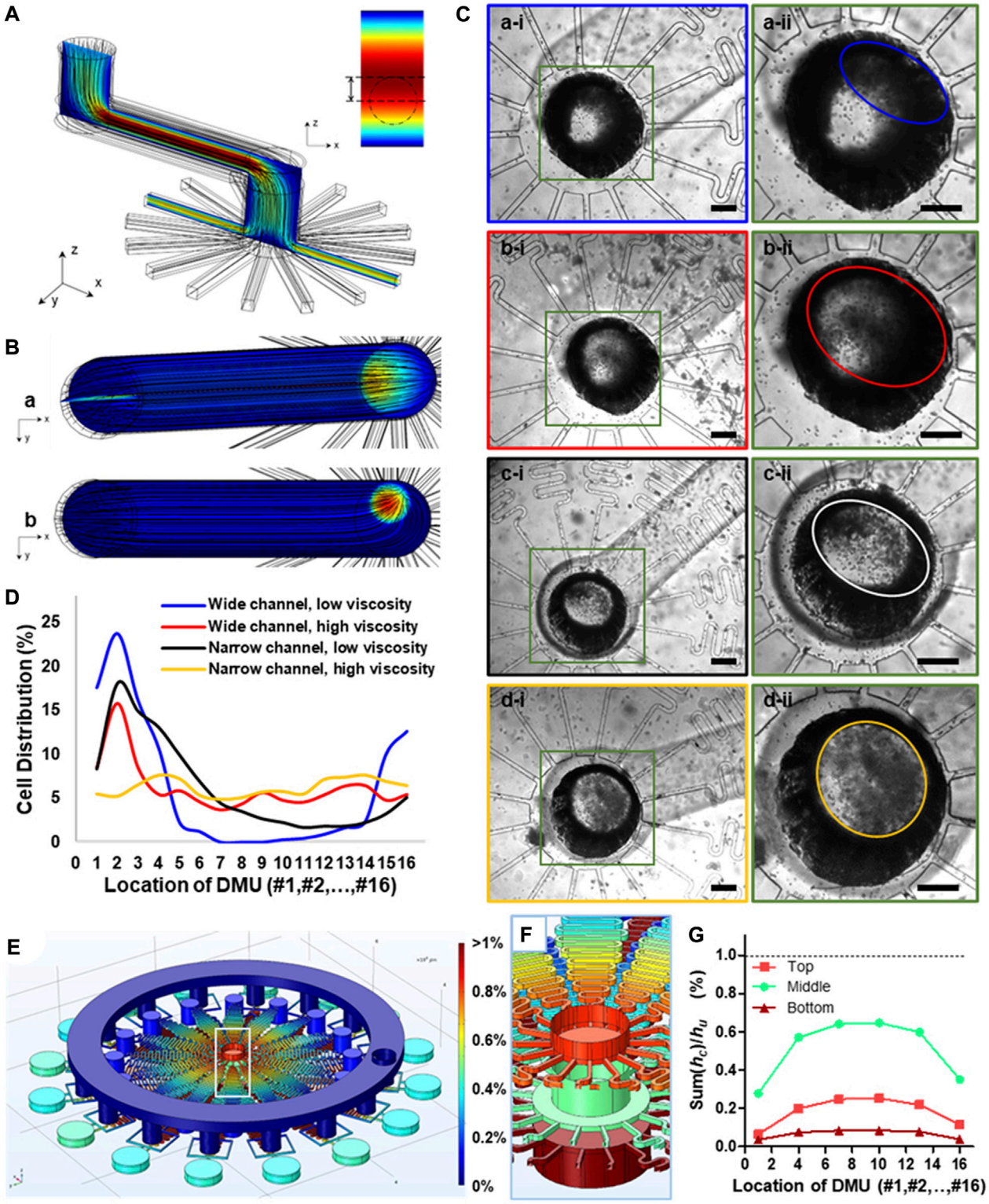

FIGURE 2
The prediction of movement state of microparticles within microchannels and the design of integrated microfluidic chip based on computational fluid simulation by COMSOL Multiphysics. **(A)** 3D structure of the partial channel structure containing one wide and long microchannel with several turns and a distribution section with 16 parallelized channels within integrated chips to predict the movement state of microparticles. **(B)** The cross-section view of fluid velocity distribution within microchannels with different channel sizes under the same flow

(*Continued*)

FIGURE 2 (Continued)
rate. **(C)** Bright-field microscopic images showing the particle distribution state within channels under the combination of wide or narrow channel and low or high fluid viscosity. The width of the wide channel was 1,000 μm, while that of the narrow channel was 500 μm. The fluid viscosity for liquid phase of low viscosity was 1 mPa·s, while that of liquid of high viscosity was 95 mPa·s. Scale bars are 300 μm. **(D)** Quantification of particle distribution in different channels under different fluid parameters. **(E)** Heat map, showing the equivalent pressure distribution of the 3D structure model of the integrated chip. **(F)** The local view of the equivalent pressure distribution of inlets of three liquid phase **(G)** Quantification of local fluid resistance Sum (h_{ci}) of collection channel downstream of each DMU in proportion to the fluid resistance of DMUs hu based on simulation results of hydraulic pressure **(E)**.

Statistical analysis

All data were presented as mean ± standard deviation. Data were analyzed by GraphPad Prism 5. Statistical differences were analyzed with the one-way analysis of variance (ANOVA) and Tukey's post hoc test. $p < 0.05$ was considered as statistically significant.

Results and discussion

Prediction of movement state of microparticles within microchannels

Conventional techniques for the microfluidic encapsulation of micrometer-sized cargoes (e.g., cells) typically rely on the high dispersity and random distribution of the microparticles dispersed in aqueous phase (Xiang et al., 2019; Kwon and Choi, 2021), which is easily to realize in the single DMU with narrow and short channels. For large-scale microfluidic encapsulation, however, wider and longer channels are needed, the sedimentation and aggregation of these micro-sized cargoes are inevitable and thus cause channel blockage and/or uneven distribution of cargoes between parallelized channels (Shao et al., 2020). Thus, to avoid cargo sedimentation and to realize even distribution between channels are the main hurdles that need to be overcome for the design and optimization of integrated microfluidic chips. Thus, we firstly aimed to predict and analyze the parameters causing cargo sedimentation in micrometer-sized channels by simulating the behavior of solid microparticles as the model in fluid. To alleviate microparticle sedimentation, the key is to balance the driving forces between gravity and buoyancy that the microparticles were exposed to, as well as the fluid viscosity of the liquid phase. Laminar flows can be formed in the microchannels which resulted in the generation of a velocity gradient along the cross-section of the channel (Figure 2A). Thus, each microparticle in the channel was exposed to significant flow rate differences surrounding the particle (Figure 2A). This would lead to the formation of an inertial lift force along the cross-section that can drive the microparticles moving to the higher flow-rate area (to the central area in the channel). The inertial lift force can be calculated by Bernoulli equation:

$$p + \frac{1}{2}\rho v^2 + \rho g h = C \tag{1}$$

where p is the hydraulic pressure at any position in the liquid phase, v is the fluid velocity at this location, ρ is the liquid density, h is the depth of this position and C is a constant, representing the conservation of energy within the same channel. Thus, the inertial lift force $\sum v$ can be calculated by the summation of hydraulic pressure p, i.e.

$$\sum v = \int_0^{\frac{\pi}{2}} \frac{1}{2}\rho v^2(-\theta) - \int_{\frac{\pi}{2}}^{\pi} \frac{1}{2}\rho v^2(\theta) \tag{2}$$

where r is the radius of microparticle, $v(\theta)$ is the fluid velocity at this position under the laminar flow. Thus, to balance the forces imposed to the microparticles, the inertial lift force $\sum v$ can be introduced to balance the gravity G and the buoyancy b to keep the microparticles from sedimentation (Supplementary Figure S1), i.e.

$$\sum v + b > G \tag{3}$$

$$\int_0^{\frac{\pi}{2}} \frac{1}{2}\rho_l v^2(-\theta) - \int_{\frac{\pi}{2}}^{\pi} \frac{1}{2}\rho_l v^2(\theta) + 2\rho_l g r > 2g\rho_p r \tag{4}$$

where ρ_l is the density of liquid phase and ρ_p is the density of micro-particle. Therefore, we can predict that higher fluid velocity gradient can effectively avoid cell sedimentation by introducing higher inertial lift force to them.

Based on this theory, we herein proposed a modified chip design based on out previously reported integrated chip (Zhang et al., 2021), which contained more than one wide and long microchannel even with several turns and a distribution section with more than 16 parallelized channels. We further investigated the specific parameters related to particle sedimentation based on computational simulation (Figure 2A). We obtained the heat maps of fluid velocity distribution within the chip, and showed obvious differences between chips of different dimensions under the same flow rate (Figure 2B). The laminar flow typically has a uniform velocity gradient distribution along the cross-section direction in straight channels, but when it flows through the corner, an uneven distribution of microparticles along the tubular channels can be observed, wherein the microparticles are more likely to concentrated at the proximal site rather than the distal site (Figure 2Ba); this will subsequently compromise the uniform cell distribution between radially parallelized channels. Meanwhile, with a narrower connection channel, the velocity

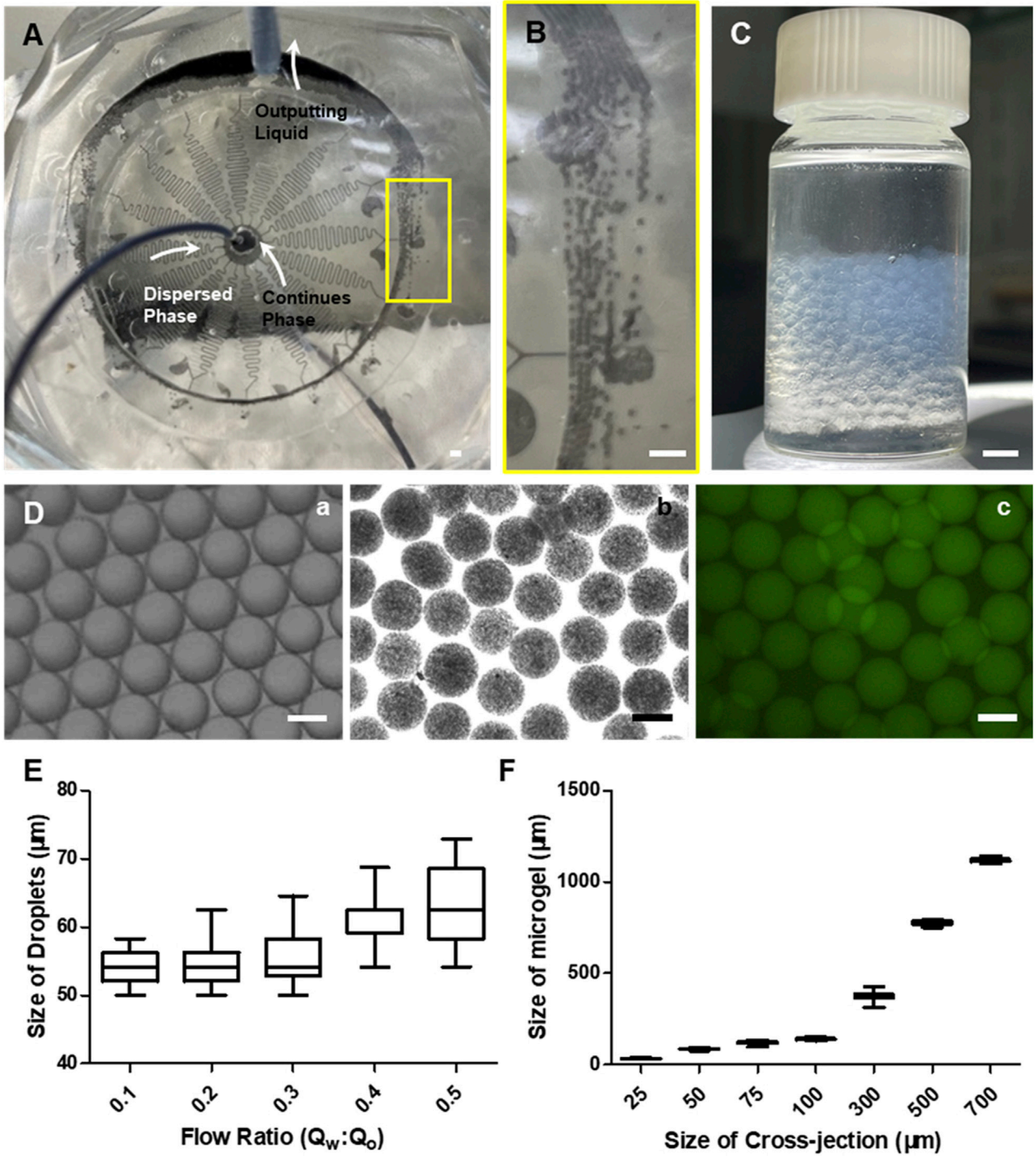

FIGURE 3
Experimental data of the integrated chip for large-scale production of alginate microgels. **(A)** Photograph showing the integrated microfluidic chip connected by inlet and outlet tubes during microgels preparation. Scale bar is 1 mm. **(B)** The local view showing the flow state of the mixture of continues phase and microgels within connection channel. Scale bar is 1 mm. **(C)** Photograph showing the output liquids collected 16× DMUs integrated chip for 5-min fabrication. Scale bar is 1 mm. **(D)** Representative bright field of microscopic images of micro-droplets **(A)** and microgels **(B)** and confocal microscopic images **(C)** for microgels generated by integrated microfluidic chips. FITC-polystyrene nanoparticles were encapsulated in microgels. Scale bars are 100 μm. **(E)** The size distribution of the resulting droplets produced with different flow rate ratios Q_{aqu}/Q_{oil} at a fixed Q_{oil} (16 ml h^{-1}). **(F)** The size distribution of the resulting microgels produced with different channel sizes at a fixed flow rate ratios Q_{aqu}/Q_{oil} (1/10).

gradient would be significant higher in the whole connection channel, and the higher velocity region tended to locate in the center of the channel and become circularly (Figure 2Bb).

We further experimentally tested our proposed microfluidic chip design for large-scale encapsulation of live cells (Figure 2C). It can be concluded that channel dimensions and precursor viscosity of the inputting fluids can significantly influence uniform distribution of cells in parallelized channels. Specifically, a wide channel dimension (a width of 1,000 μm) and low-viscosity disperse phase (1 mPa·s) was more likely to induce flow uneven distribution in the centered inputting channel (Figure 2Ca-ii); this led to a considerably heterogeneous distribution of cells between parallelized channels. This experimental observation was in line with our computation simulation wherein cell-mimicking microparticles also showed uneven distribution between DMUs using these parameters (Figure 2Ba). By counting the number of cells in the parallelized channels, we quantified the uniformity of cell distribution under these parameters (coefficient of variability, CV = 123.87%, Figure 2D, blue line). In contrast, with a narrow channel (500 μm) and the same flow viscosity, the ellipticity of cells distribution region is become smaller (Figure 2Cc-ii), and the cells distribution was also relatively more uniform than larger channel (CV = 82.91%, Figure 2D, black line). Moreover, we further investigated the effect of the viscosity of the disperse phase containing live cells suspended in hydrogel precursor, and found that the higher fluid viscosity (95 mPa·s) can improve the uniformity of cells dispersion in both large or small microchannels. Especially, combination with narrower channel dimension and enhanced precursor viscosity almost completely alleviated the heterogeneity of cell distribution between DMUs (Figure 2Cd-ii), evidenced by CV = 15.51% (Figure 2D, yellow line); this is of significant importance for continuous and scale-up preparation cell-laden microgels with the same parameters.

Optimization of chip design based on computational simulation

We further optimized the design of integrated chip containing multiple parallelized DMUs for scale-up production of cell-laden microgels. In our previous work (Zhang et al., 2022), we designed a radially parallelized device to ensure all liquids are apportioned equally, avoiding the decay of flow rate between each DMU. However, this design was not capable of generating droplets or microgels with multiple components. Besides, the unidirectionally annular collection channel sometimes will suffer from regurgitation due to high pressure of the collection channel or blockage of individual DMU. Therefore, we herein optimized the microchannel's structure and decreased the coupling degree between DMUs (Figure 2E). Specifically, we used a larger annular channel as the collection channel to allow faster collection and removal of the large amount of produced microgels, and used parallelized and independent DMUs to produce microgels independently to avoid the interference induced by the blockage of neighboring DMUs.

To further ensure the uniform distribution between parallelized channels and maintain high flow velocity, we need to keep the sum of fluid resistance h_{ci} in the collection channels significantly lower than the fluid resistance h_u of each DMUs, i.e., Sum $(h_{ci})/h_u$ < 1% (Zhang et al., 2022). Meanwhile, for multiple liquid phase injection with different flow rate, the fluid resistances h_{ul} of each DMUs for different liquid phases were also different. Thus, the requirement of fluid resistance h_{ci} in the collection channels should be significantly lower than the minimum fluid resistance h_{umin} of each DMUs, i.e., Sum $(h_{ci})/h_{umin}$ < 1% (Supplementary Figure S2).

To optimize the channel design, we simulated the fluid behavior in the microfluidic chip using CFD simulation. The hydraulic pressure at the outlet of the collection channel has the minimal value, p_{min}, which was set at $p_{min} = 0$, and the inlet of oil phase has the maximal hydraulic pressure $p_{max.}$ To simplify the calculation, the hydraulic pressure p in anywhere inside the channel was homogenized by p_{max} (i.e., $p_{max} = 1$). Thus, the fluid resistance h of any section of the channel can be expressed by the hydraulic pressure difference Δp between the initial and final ends of this section of this channel. We obtained the heat maps of hydraulic pressure p within the whole 3D chip model. Particularly, the chip model was used for Janus-microgel preparation; thus, it had three inputting liquid phases with different flow rates, and showing different hydraulic pressure at their inlets (Figure 2F). The heat map showed homogeneous distribution of hydraulic pressure within collection channels, evidenced by the quantified ratio of Sum $(h_{ci})/h_u$ for each liquid phase was less than 1% (Figure 2G). In general, our result from computational simulation demonstrated the stability and reliability of our integrated chips for scale-up microgel generation.

Experimental demonstration of the large-scale generation of droplets and microgels

We further evaluated the performance of the optimized chip containing 16 DMUs for generating alginate microgels with different size and complex structures such as Janus or core-shell microgels (Figures 1C,D, 3A). Based on the geometry structure of DMUs, droplets can be produced and preformed within the cross-junctions, thereafter triggering on-chip gelation to solidify the complex structure of Janus or core-shell structure (Supplementary Figure S4). The collection of the resulting microparticles was similar as previously reported design (Figures 3B,C, Supplementary Video S1) (Zhang et al., 2022). We further tested the operation parameters of the integrated chip based on a stable emulsion system containing a HFE7100 continuous phase with amphiphilic triblock

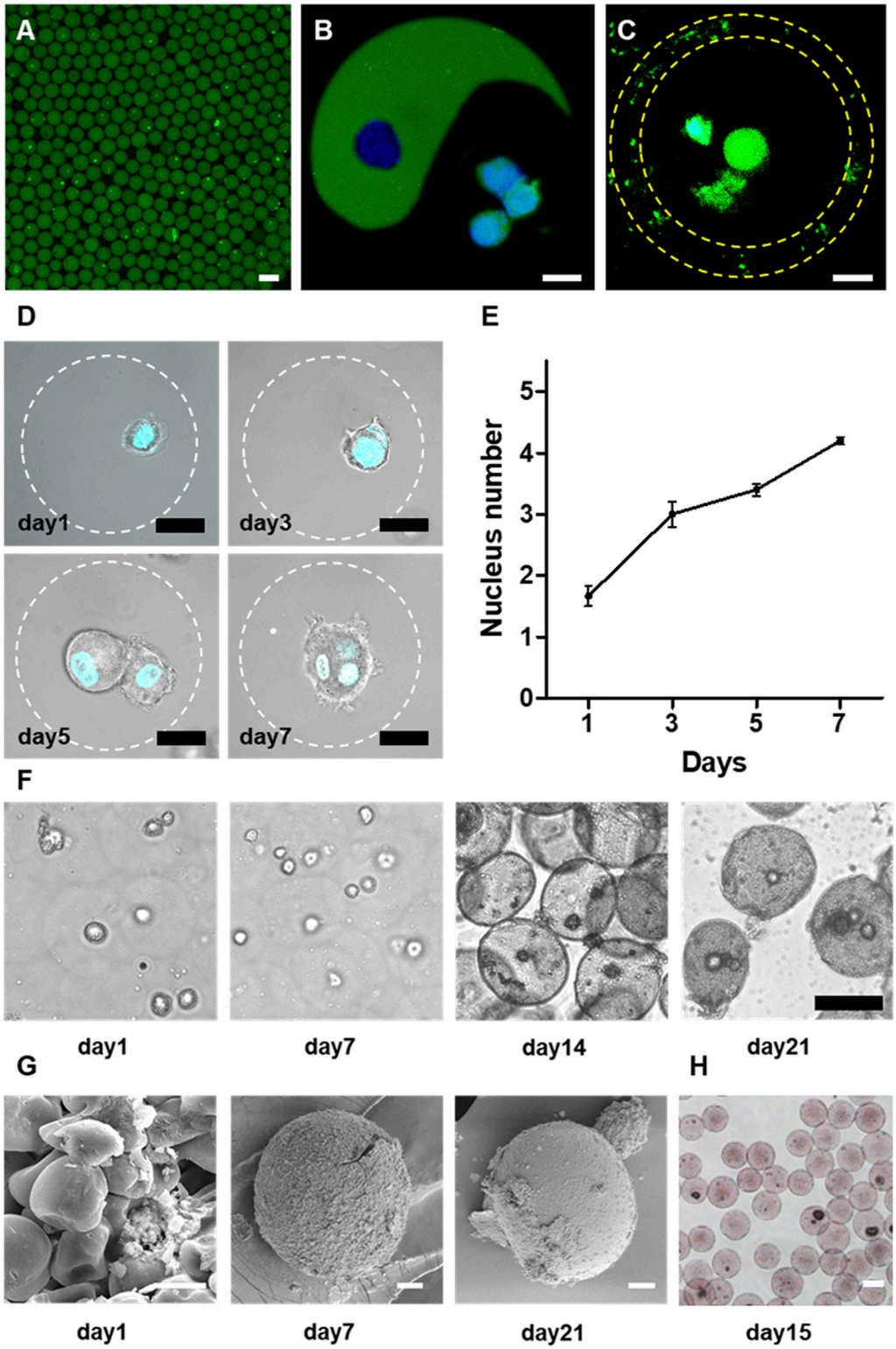

FIGURE 4
One-step microfluidic approach for large-scale generation of cell-laden microgels. **(A)** The representative confocal microscopic image of the rat bone marrow stromal cells (MSCs) encapsulated in alginate microgels. Alginate was labeled by fluorescein and cells were marked by GFP. Scale bar is 100 μm.,**(B,C)** The representative confocal microscopic images of rat-MSCs encapsulated in Janus **(B)** and Core-shell **(C)** alginate microgels. Scale bars are 20 μm. **(D)** The confocal microscopic images of MSCs in the microgels. Cells were stained by DAPI nuclei staining. Cells

(*Continued*)

FIGURE 4 (Continued)
proliferated continuously within the microgels, evidenced by the growth of cell numbers within the microgels. Scale bars are 20 μm. **(E)** Quantification of nucleus number within one microgel during 7 days culture. **(F)** Representative light microscopic images of encapsulated rat MSCs in alginate microgels upon osteogenic culture. Due to calcium phosphate deposition, the microgels gradually became opaque. Scale bars are 50 μm. **(G)** SEM images showing the microstructure of cell-laden microgels at different time points during the osteogenic culture. Scale bars are 10 μm. **(H)** Alizarin red staining of cell-laden microgels after 15 days of osteogenic culture suggesting the mineralization of the alginate matrix. Scale bar is 50 μm.

copolymer surfactant (An et al., 2021) and a pure water dispersed phase (Figure 3Da). Droplets with a narrower size distribution can be obtained with a relatively low flow rate ratio evidenced by the CV values lower than 4% for Q_{aqu}/Q_{oil} < 1:2.5, while a higher flow rate ratio Q_{aqu}/Q_{oil} caused wider size distribution (CV = 6.67% for Q_{aqu}/Q_{oil} = 1:2, Figure 3E). Considering the limited flow rate of aqueous phase to avoid to generate high shear force upon cell encapsulation, we maintained a low flow rate ratio of Q_{aqu}/Q_{oil} = 1:10 for microgels generation in the integrated chip with different sizes. This allowed the generation of alginate microgels with a narrower size distribution (CV < 5%) under different size (Figure 3D, Fb, c), and the maximum production throughput can be achieved up to 240 ml/h (Supplementary Video S2).

Microfluidic encapsulation of live cells using the integrated chip

We further used these different microfluidic devices for the generation of MSC-laden microgels of different microstructures. Alginate conjugated with cell attachment motif (arginine-glycine-aspartic acid, RGD) was used to ensure cell attachment and their functionality (Chen et al., 2016; Zhang et al., 2022). MSCs dispersed in alginate precursor solution was used as the input disperse phase and was then encapsulated into spherical alginate microgels based on the above-mentioned process (Figure 4A). For the preparation of MSCs-laden Janus microgels, specific DMU design with two aqueous phase inlets (Supplementary Figure S3B) (Zhang et al., 2018) was used instead of the conventional cross-junction structure, and two MSC-containing suspensions were introduced with the same flow rate to form dual-compartmentalized microgels with both sites loaded with MSCs separately (Figure 4B). For the preparation of core-shell microgels, we designed the DMU with two sequential cross-junctions to allow firstly cell-encapsulation and secondly gelation of the shell layer (Supplementary Figure S3C) (Choi et al., 2016) (Figure 4C).

To evaluate the long-term viability of encapsulated cells, we encapsulated MSCs into monodisperse spherical microgels and cultured them for 7 days. We observed continuous proliferation of encapsulated cells in alginate microgels during *in vitro* culture (Figure 4D). The encapsulated cells maintained a relatively spherical shape in RGD-alginate matrix during the 3D culture due to the high stiffness of alginate that restricted cell movement and spreading[34,36]. Even though, the proliferation of MSCs can be demonstrated by quantification of the average nuclei number of the entrapped cell clusters (Figures 4D,E). It was revealed that the majority of cell-laden microgels initially contained single cells after encapsulation, which gradually proliferated to form spheroids containing multiple cells after couple of days.

We further investigated the functionality of encapsulated MSCs by assessing the osteogenic capacity of the MSCs within the microgels cultured in osteogenic medium (An et al., 2020). The encapsulated MSCs were demonstrated to commit to the osteogenic lineage as evidenced by the induced mineralization of the microgel matrix. The initially transparent alginate microgels gradually turned into opaque after 3 weeks of osteogenic culture. The microscopic images revealed that the majority of the microgels (especially those containing cells) showed gradually increased opacity due to the mineral deposition (Figure 4F). Specifically, most cell-laden alginate microgels showed more opacity compared to empty microgels at the early stage upon the inductive culture (Figure 4F), indicating that the encapsulated MSCs may play a pivot role in triggering the mineralization process. Further SEM images confirmed the gradual mineralization of the microgel matrix as reflected by the transformation from an initially deformable polymeric network into a composite matrix with densely packed calcium phosphate particles embedded in the hydrogel matrix (Figure 4G). Further analysis of the composition of the precipitated minerals by element mapping using alizarin red staining for calcium deposition indicated the precipitation of calcium phosphate (CaP) minerals in the gel matrix (Figure 4H). These findings suggested that the alginate microgels provided a spatially confined but physiologically relevant microenvironment to support cell viability, proliferation, and long-term functionality. More importantly, we demonstrated the biocompatibility of the current integrated microfluidic devices, and the feasibility of this approach for scalable high-throughput generation of cell-laden microgels.

Conclusion

We herein presented the design and optimization of integrated microfluidic chip for large-scale preparation of

cell-laden microgels with controllable size and complex microstructure. We investigated the mechanism of cell sedimentation and uneven distribution in radially parallelized microchannel, and optimized the operation parameters to address these problematic issues. It was demonstrated that the higher fluid velocity gradient and higher fluid viscosity can alleviate the cell sedimentation and aggregation in the microchannel and provide more uniform cell distribution between parallelized channels. Moreover, we designed multiple-layered microfluidic chips allowing multiple inputting liquids for the fabrication of microgels with complex structures. This integrated chip facilitated cell encapsulation at a maximum production rate of 240 ml/h of cell suspension with retained cell viability and functionality. In general, the current microfluidic strategy represents a significant step forward for scale-up encapsulation technology and could offer a potentially viable option for practical applications of cell-laden microgels in cell therapies, tissue engineering and clinical application.

Data availability statement

The original contributions presented in the study are included in the article/Supplementary Material, further inquiries can be directed to the corresponding author.

Author contributions

HZ and HW. designed the research; HZ, CL, YZ, CA, HL, JY, and YHZ.performed research; HZ, WH, and HN; HZ and HW. wrote the paper.

Funding

This work is supported by the National Key Research and Development Program of China (No. 2018YFA0703000), the National Natural Science Foundation of China (No.31870957), the Fundamental Research Funds for the Central Universities (No. DUT20YG103 and DUT22LAB601), the Innovation Foundation of Science and Technology of Dalian (No. 2021JJ13SN49), and Shenzhen Basic Research Program general project (JCYJ20190808152211686 and JCYJ20190808120217133).

Conflict of interest

The authors declare that the research was conducted in the absence of any commercial or financial relationships that could be construed as a potential conflict of interest.

Publisher's note

All claims expressed in this article are solely those of the authors and do not necessarily represent those of their affiliated organizations, or those of the publisher, the editors and the reviewers. Any product that may be evaluated in this article, or claim that may be made by its manufacturer, is not guaranteed or endorsed by the publisher.

Supplementary material

The Supplementary Material for this article can be found online at: https://www.frontiersin.org/articles/10.3389/fsens.2022.1037723/full#supplementary-material

References

Amstad, E., Chemama, M., Eggersdorfer, M., Arriaga, L. R., Brenner, M. P., and Weitz, D. A. (2016). Robust scalable high throughput production of monodisperse drops. *Lab. Chip* 16, 4163–4172. doi:10.1039/c6lc01075j

An, C., Liu, W., Zhang, Y., Pang, B., Liu, H., Zhang, Y., et al. (2020). Continuous microfluidic encapsulation of single mesenchymal stem cells using alginate microgels as injectable fillers for bone regeneration. *Acta Biomater.* 111, 181–196. doi:10.1016/j.actbio.2020.05.024

An, C., Zhang, Y., Li, H., Zhang, H., Zhang, Y., Wang, J., et al. (2021). Thermo-responsive fluorinated surfactant for on-demand demulsification of microfluidic droplets. *Lab. Chip* 21, 3412–3419. doi:10.1039/d1lc00450f

Chen, Q., Utech, S., Chen, D., Prodanovic, R., Lin, J. M., and Weitz, D. A. (2016). Controlled assembly of heterotypic cells in a core–shell scaffold: Organ in a droplet. *Lab. Chip* 16, 1346–1349. doi:10.1039/c6lc00231e

Choi, C. H., Wang, H., Lee, H., Kim, J. H., Zhang, L., Mao, A., et al. (2016). One-step generation of cell-laden microgels using double emulsion drops with a sacrificial ultra-thin oil shell. *Lab. Chip* 16, 1549–1555. doi:10.1039/c6lc00261g

Conchouso, D., Castro, D., Khan, S. A., and Foulds, I. G. (2014). Three-dimensional parallelization of microfluidic droplet generators for a litre per hour volume production of single emulsions. *Lab. Chip* 14, 3011–3020. doi:10.1039/c4lc00379a

Femmer, T., Jans, A., Eswein, R., Anwar, N., Moeller, M., Wessling, M., et al. (2015). High-throughput generation of emulsions and microgels in parallelized microfluidic drop-makers prepared by rapid prototyping. *ACS Appl. Mat. Interfaces* 7, 12635–12638. doi:10.1021/acsami.5b03969

Griffin, D. R., Archang, M. M., Kuan, C. H., Weaver, W. M., Weinstein, J. S., Feng, A. C., et al. (2020). Activating an adaptive immune response from a hydrogel scaffold imparts regenerative wound healing. *Nat. Mater* 20, 560–569. doi:10.1038/s41563-020-00844-w

Griffin, D. R., Weaver, W. M., Scumpia, P. O., Di Carlo, D., and Segura, T. (2015). Accelerated wound healing by injectable microporous gel scaffolds assembled from annealed building blocks. *Nat. Mat.* 14, 737–744. doi:10.1038/nmat4294

Hati, A. G., Szymborski, T. R., Steinacher, M., and Amstad, E. (2018). Production of monodisperse drops from viscous fluids. *Lab. Chip* 18, 648–654. doi:10.1039/c7lc01322a

Jeong, H.-H., Issadore, D., and Lee, D. (2016). Recent developments in scale-up of microfluidic emulsion generation via parallelization. *Korean J. Chem. Eng.* 33, 1757–1766. doi:10.1007/s11814-016-0041-6

Jeong, H. H., Yadavali, S., Issadore, D., and Lee, D. (2017). Liter-scale production of uniform gas bubbles via parallelization of flow-focusing generators. *Lab. Chip* 17, 2667–2673. doi:10.1039/c7lc00295e

Jeong, H. H., Yelleswarapu, V. R., Yadavali, S., Issadore, D., and Lee, D. (2015). Kilo-scale droplet generation in three-dimensional monolithic elastomer device (3D MED). *Lab. Chip* 15, 4387–4392. doi:10.1039/c5lc01025j

Khan, M., Mao, S., Li, W., and Lin, J. (2018). Microfluidic devices in the fast-growing domain of single-cell analysis. *Chem. Eur. J.* 24, 15398–15420. doi:10.1002/chem.201800305

Kwon, T., and Choi, K. (2021). Separation of ultra-high-density cell suspension via elasto-inertial microfluidics. *J. Han. Small* 17, e2101880. doi:10.1002/smll.202101880

Li, W., Zhang, L., Ge, X., Xu, B., Zhang, W., Qu, L., et al. (2018). Microfluidic fabrication of microparticles for biomedical applications. *Chem. Soc. Rev.* 47, 5646–5683. doi:10.1039/c7cs00263g

Mao, A. S., Ozkale, B., Shah, N. J., Vining, K. H., Descombes, T., Zhang, L., et al. (2019). Programmable microencapsulation for enhanced mesenchymal stem cell persistence and immunomodulation. *Proc. Natl. Acad. Sci. U. S. A.* 116, 15392–15397. doi:10.1073/pnas.1819415116

Mao, A. S., Shin, J. W., Utech, S., Wang, H., Uzun, O., Li, W., et al. (2017). Deterministic encapsulation of single cells in thin tunable microgels for niche modelling and therapeutic delivery. *Nat. Mat.* 16, 236–243. doi:10.1038/nmat4781

Martins, E., Poncelet, D., Rodrigues, R. C., and Renard, D. (2017). Oil encapsulation techniques using alginate as encapsulating agent: Applications and drawbacks. *J. Microencapsul.* 34, 754–771. doi:10.1080/02652048.2017.1403495

Montessori, A., Lauricella, M., Succi, S., Stolovicki, E., and Weitz, D. (2018). Elucidating the mechanism of step emulsification. *Phys. Rev. Fluids* 3, 072202. doi:10.1103/physrevfluids.3.072202

Nawar, S., Stolaroff, J. K., Ye, C., Wu, H., Nguyen, D. T., Xin, F., et al. (2020). Parallelizable microfluidic dropmakers with multilayer geometry for the generation of double emulsions. *Lab. Chip* 20, 147–154. doi:10.1039/c9lc00966c

Nisisako, T., Ando, T., and Hatsuzawa, T. (2012). High-volume production of single and compound emulsions in a microfluidic parallelization arrangement coupled with coaxial annular world-to-chip interfaces. *Lab. Chip* 12, 3426–3435. doi:10.1039/c2lc40245a

Nisisako, T., and Torii, T. (2008). Microfluidic large-scale integration on a chip for mass production of monodisperse droplets and particles. *Lab. Chip* 8, 287–293. doi:10.1039/b713141k

Ofner, A., Moore, D. G., Rühs, P. A., Schwendimann, P., Eggersdorfer, M., Amstad, E., et al. (2017). High-throughput step emulsification for the production of functional materials using a glass microfluidic device. *Macromol. Chem. Phys.* 218, 1600472. doi:10.1002/macp.201600472

Romanowsky, M. B., Abate, A. R., Rotem, A., Holtze, C., and Weitz, D. A. (2012). High throughput production of single core double emulsions in a parallelized microfluidic device. *Lab. Chip* 12, 802–807. doi:10.1039/c2lc21033a

Shao, F., Yu, L., Zhang, Y., An, C., Zhang, H., Zhang, Y., et al. (2020). Microfluidic encapsulation of single cells by alginate microgels using a trigger-gellified strategy. *Front. Bioeng. Biotechnol.* 8, 583065. doi:10.3389/fbioe.2020.583065

Stolovicki, E., Ziblat, R., and Weitz, D. A. (2017). Throughput enhancement of parallel step emulsifier devices by shear-free and efficient nozzle clearance. *Lab. Chip* 18, 132–138. doi:10.1039/c7lc01037k

Xiang, N., Wang, J., Li, Q., Han, Y., Huang, D., and Ni, Z. (2019). Precise size-based cell separation via the coupling of inertial microfluidics and deterministic lateral displacement. *Anal. Chem.* 91, 10328–10334. doi:10.1021/acs.analchem.9b02863

Yadavali, S., Jeong, H. H., Lee, D., and Issadore, D. (2018). Silicon and glass very large scale microfluidic droplet integration for terascale generation of polymer microparticles. *Nat. Commun.* 9, 1222. doi:10.1038/s41467-018-03515-2

Youn, W., Kim, J. Y., Park, J., Kim, N., Choi, H., Cho, H., et al. (2020). Single-cell nanoencapsulation: From passive to active shells. *Adv. Mat.* 32, e1907001. doi:10.1002/adma.201907001

Zhang, H., Zhang, L., An, C., Zhang, Y., Shao, F., Gao, Y., et al. (2022). Large-scale single-cell encapsulation in microgels through metastable droplet-templating combined with microfluidic-integration. *Biofabrication* 14, 035015. doi:10.1088/1758-5090/ac7168

Zhang, L., Chen, K., Zhang, H., Pang, B., Choi, C. H., Mao, A. S., et al. (2018). Microfluidic templated multicompartment microgels for 3D encapsulation and pairing of single cells. *Small* 14, 55. doi:10.1002/smll.201702955

Zhang, Y., An, C., Zhang, Y., Zhang, H., Mohammad, A. F., Li, Q., et al. (2021). Microfluidic-templating alginate microgels crosslinked by different metal ions as engineered microenvironment to regulate stem cell behavior for osteogenesis. *Mater. Sci. Eng. C* 131, 112497. doi:10.1016/j.msec.2021.112497

Zhao, C. X. (2013). Multiphase flow microfluidics for the production of single or multiple emulsions for drug delivery. *Adv. Drug Deliv. Rev.* 65, 1420–1446. doi:10.1016/j.addr.2013.05.009

Zhu, P., and Wang, L. (2016). Passive and active droplet generation with microfluidics: A review. *Lab. Chip* 17, 34–75. doi:10.1039/c6lc01018k